NASA Technical Paper 3380

July 1993

IN-20
179488
p-14

Hot-Gas-Side Heat Transfer Characteristics of Subscale, Plug-Nozzle Rocket Calorimeter Chamber

Richard J. Quentmeyer
and Elizabeth A. Roncace

(NASA-TP-3380) HOT-GAS-SIDE HEAT TRANSFER CHARACTERISTICS OF SUBSCALE, PLUG-NOZZLE ROCKET CALORIMETER CHAMBER (NASA) 14 p

N94-12569

Unclas

H1/20 0179488

NASA

NASA
Technical
Paper
3380

1993

Hot-Gas-Side Heat Transfer Characteristics of Subscale, Plug-Nozzle Rocket Calorimeter Chamber

Richard J. Quentmeyer
and Elizabeth A. Roncace
Lewis Research Center
Cleveland, Ohio

NASA
National Aeronautics and
Space Administration
Office of Management
Scientific and Technical
Information Program

Hot-Gas-Side Heat Transfer Characteristics of Subscale, Plug-Nozzle Rocket Calorimeter Chamber

Richard J. Quentmeyer
Sverdrup Technology, Inc.
Lewis Research Center Group
Brook Park, Ohio

and

Elizabeth A. Roncace
NASA Lewis Research Center
Cleveland, Ohio

Summary

An experimental investigation was conducted to determine the hot-gas-side heat transfer characteristics for a liquid-hydrogen-cooled, subscale, plug-nozzle rocket test apparatus. This apparatus has been used since 1975 to evaluate rocket engine advanced cooling concepts and fabrication techniques, to screen candidate combustion chamber liner materials, and to provide data for model development. In order to obtain the data, a water-cooled calorimeter chamber having the same geometric configuration as the plug-nozzle test apparatus was tested. It also used the same two showerhead injector types that have been used on the test apparatus: one having a Rigimesh faceplate and the other having a platelet faceplate. The tests were conducted using liquid oxygen and gaseous hydrogen as the propellants over a mixture ratio range of 5.8 to 6.3 at a nominal chamber pressure of 4.14 MPa abs (600 psia). The two injectors showed similar performance characteristics with the Rigimesh faceplate having a slightly higher average characteristic-exhaust-velocity efficiency of 96 percent versus 94.4 percent for the platelet faceplate. The throat heat flux was 54 MW/m^2 (33 Btu/in.^{2}-sec) at the nominal operating condition, which was a chamber pressure of 4.14 MPa abs (600 psia), a hot-gas-side wall temperature of 730 K (1314 °R), and a mixture ratio of 6.0. The chamber throat region correlation coefficient C_g for a Nusselt number correlation of the form $Nu = C_g(Re)^{0.8}(Pr)^{0.3}$ averaged 0.023 for the Rigimesh faceplate and 0.026 for the platelet faceplate.

Introduction

In a continuing effort to provide new technology for improving existing rocket engines and creating long-life, low-cost designs for future rocket engines, NASA has used a subscale, plug-nozzle rocket test apparatus to evaluate advanced cooling concepts and fabrication techniques, to screen candidate combustion chamber liner materials, and to provide data for model development (refs. 1 to 10). The test apparatus consists of an annular injector; a water-cooled, contoured centerbody that forms the combustion chamber, throat, and nozzle sections; and a liquid-hydrogen-cooled outer chamber that serves as the test section (fig. 1).

During this ongoing program, tests have been conducted using two types of showerhead injectors: one having a Rigimesh faceplate and the other having a platelet faceplate. All tests have been conducted using liquid oxygen and gaseous hydrogen as the propellants. Figure 2 shows the test apparatus during cyclic testing.

The hot-gas-side heat transfer boundary conditions are required for performing thermal and structural analyses on the test chambers. In order to provide these data, a water-cooled calorimeter chamber having the same geometric configuration as the plug-nozzle test apparatus was fabricated and tested. Tests were conducted for both injector types using liquid oxygen and gaseous hydrogen as the propellants over a mixture range of 5.8 to 6.3 at a nominal chamber pressure of 4.14 MPa

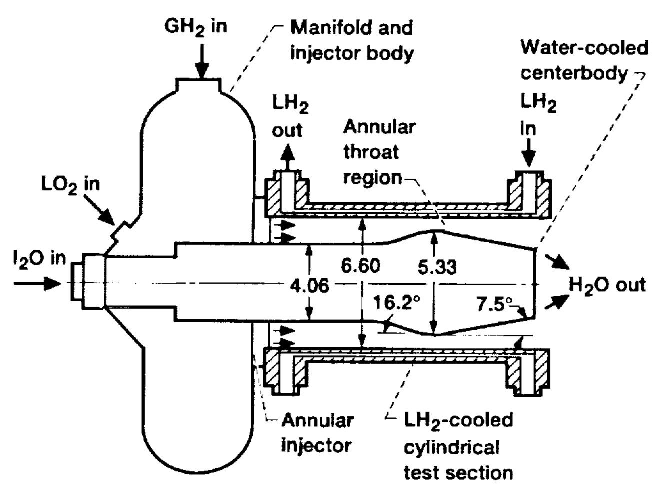

Figure 1.—Schematic of plug-nozzle rocket engine test apparatus. (Dimensions are in centimeters.)

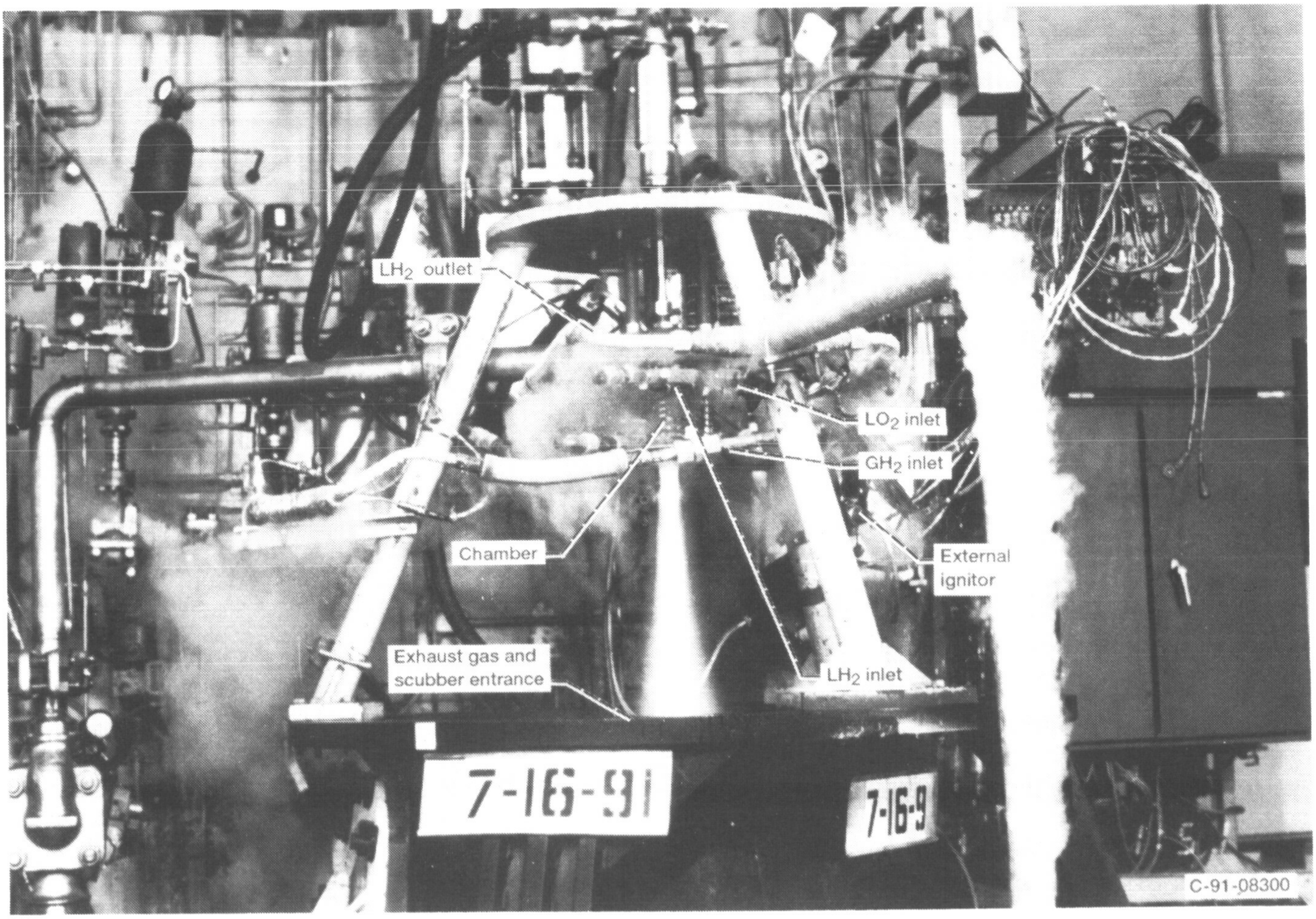

Figure 2.—Plug-nozzle rocket engine test apparatus during cyclic testing.

abs (600 psia). These are the same operating conditions used for the liquid-hydrogen-cooled test chambers.

Although the plug-nozzle test chambers have been used as an evaluation test apparatus since 1975 and numerous reports on the results have been published, the hot-gas-side heat transfer data from the calorimeter chamber have never been published. Therefore, the experimental results from the calorimeter chamber are being reported herein to provide the heat transfer characteristics of this type of apparatus.

Apparatus and Test Procedure

Calorimeter Chamber Assembly

Figure 3 shows a schematic of the calorimeter chamber assembly. The apparatus had the identical geometry as the plug-nozzle test apparatus and consisted of the annular injector; the contoured centerbody that formed the combustion chamber, throat, and nozzle sections of the thrust chamber; and the outer calorimeter chamber. The configuration had a contraction and expansion area ratio of 1.79 and a contraction half-angle of 16.2°. Liquid oxygen and gaseous hydrogen were used as the propellants at a nominal mixture ratio of 6.0 and a nominal chamber pressure of 4.14 MPa abs (600 psia), which produced a thrust of approximately 5.34 kN (1200 lbf).

Injectors.—Two injectors were evaluated in this program; both were designed to operate with liquid oxygen and gaseous hydrogen. With both injectors the oxygen was injected through 70 showerhead tubes arranged in two circular rows, 36 in the inner row and 34 in the outer row. The tubes were made of 0.23-cm-o.d. (0.091-in.) stainless steel having a 0.03-cm-thick (0.012-in.) wall. Two chamber-pressure taps were located in the outer row of oxidizer tubes.

In one injector, shown in figure 4, all of the gaseous hydrogen was injected through a porous Rigimesh faceplate. The faceplate was fabricated by sintering together a 12-layer stack of 12×64 wire-mesh plates, having a permeability of 26.9 std m^3/min (950 std ft^3/min) at 13.79 kPa (2 psid) over a 0.093-m^2 (1-ft^2) area of the plate (ref. 11). By careful selection of the

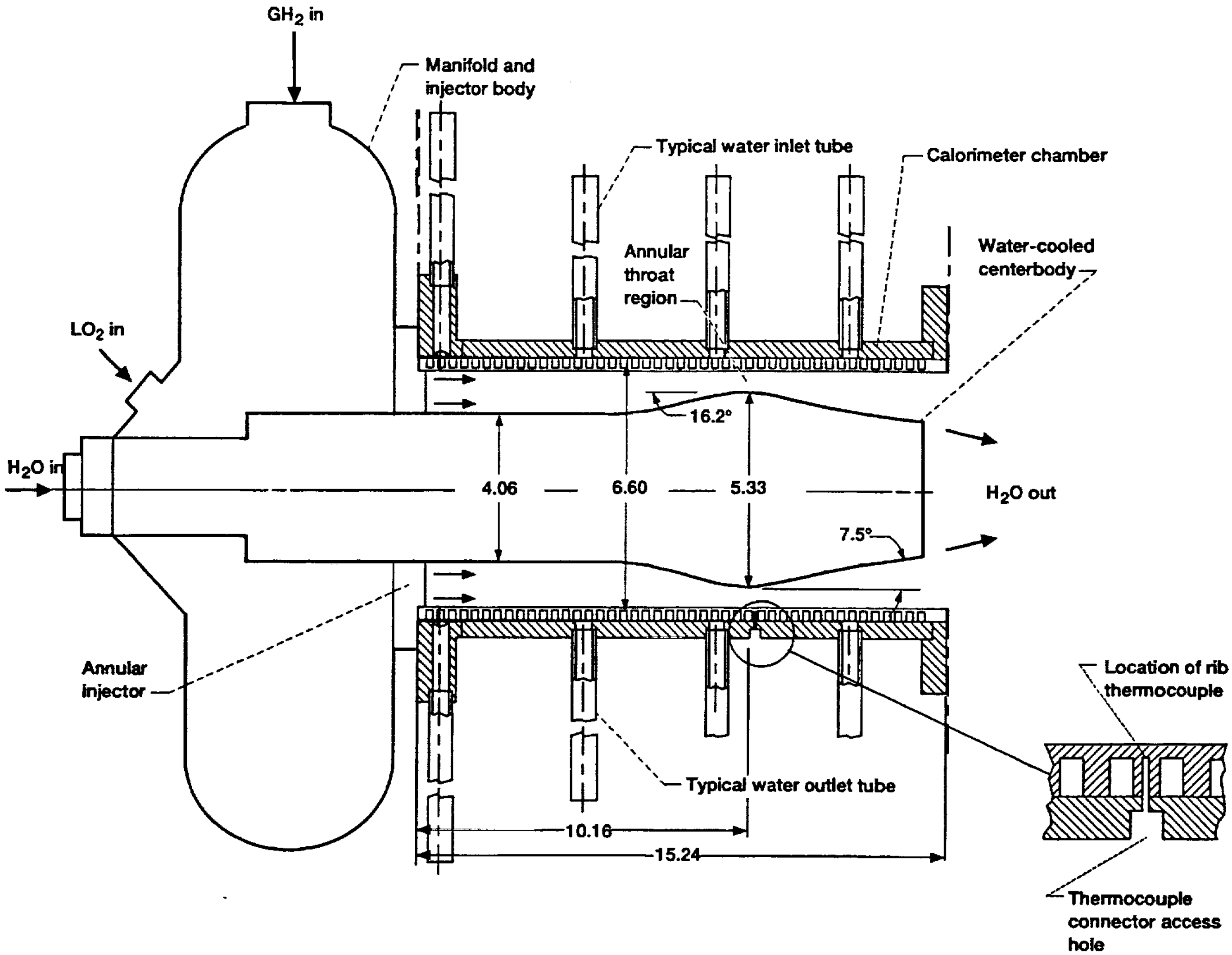

Figure 3.—Schematic of calorimeter chamber assembly. (Dimensions are in centimeters.)

mesh size and the number of layers used, the faceplate could be fabricated with a predetermined permeability. The faceplate was removable, so that it could be replaced if damaged.

In the second injector the gaseous hydrogen was injected through a porous platelet faceplate, which is shown in figure 5. The faceplate consisted of a 44-layer stack of platelets that were diffusion bonded together. Sixteen of the platelets were 0.013 cm (0.005 in.) thick, and 28 platelets were 0.025 cm (0.010 in.) thick. The combustion-side platelet had approximately 5400 photoetched holes with a diameter of 0.025 cm (0.010 in.). The holes were equally spaced between the 70 showerhead tubes for faceplate cooling and to distribute the hydrogen uniformly across the injector face. The size and number of the holes were selected to match the pressure drop of the Rigimesh faceplate (ref. 11). This faceplate was also removable.

Centerbody.—The water-cooled, contoured centerbody was fabricated from copper and had 40 rectangular cooling passages running axially throughout its length. The diameter was 4.06 cm (1.60 in.) in the combustion zone and 5.33 cm (2.10 in.) at the throat. The centerbody was 15.24 cm (6.00 in.) long with a 16.2° half-angle convergence section and a 7.5° half-angle conical expansion section. It was inserted through the injector and bolted into place from the back side. Figure 6 shows the centerbody in a cutaway of the subscale, plug-nozzle rocket test apparatus.

A 0.076- to 0.127-mm (0.003- to 0.005-in.) zirconia-oxide coating was applied to the centerbody by conventional plasma-spray techniques to reduce the heat load and to prolong the centerbody life. Water entered the centerbody from behind the injector, passed through the cooling passages, and was dumped at the thrust chamber exit.

Calorimeter chamber.—The calorimeter chamber was 15.24 cm (6.00 in.) in length and had an inside diameter of 6.6 cm (2.60 in.). The chamber was fabricated from oxygen-free, high-conductivity copper with machined circumferential

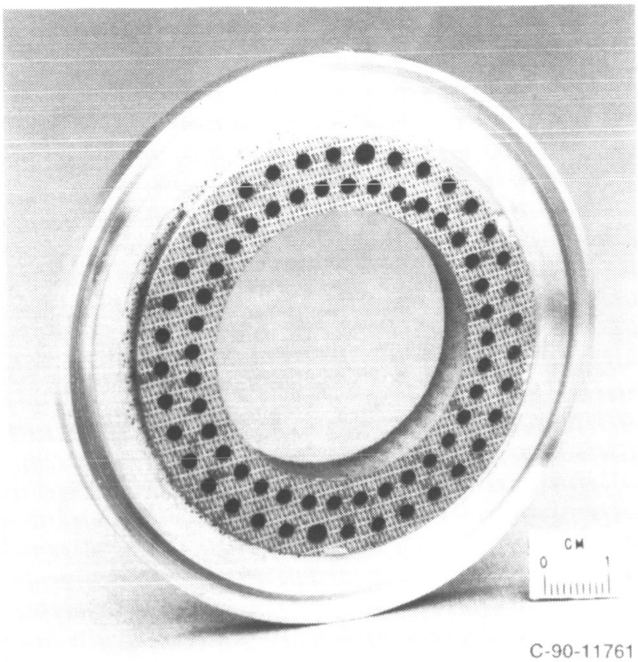

Figure 4.—Porous Rigimesh faceplate.

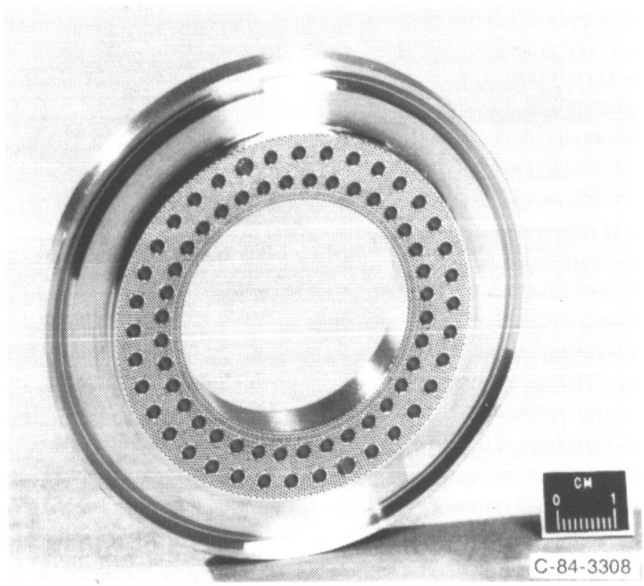

Figure 5.—Porous platelet faceplate.

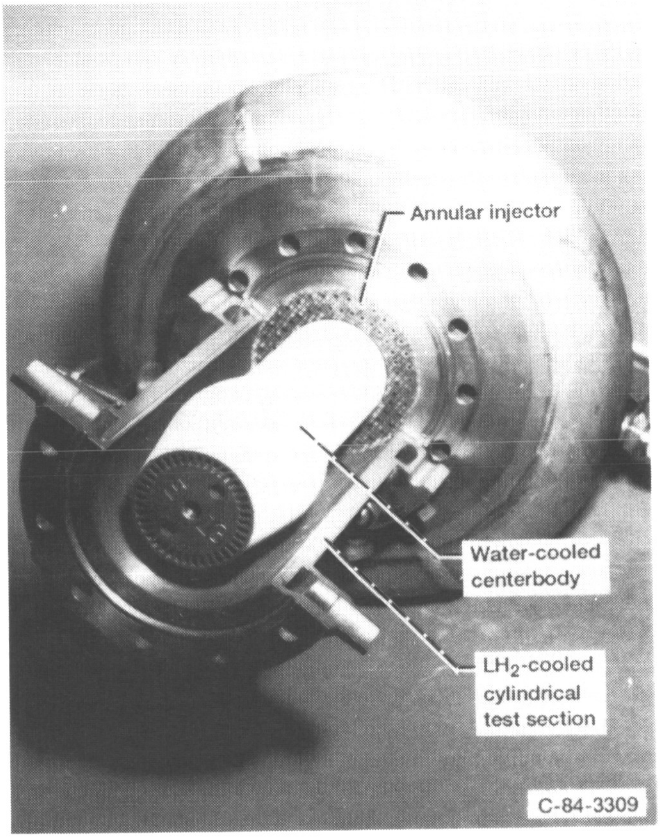

Figure 6.—Cutaway of plug-nozzle rocket test apparatus.

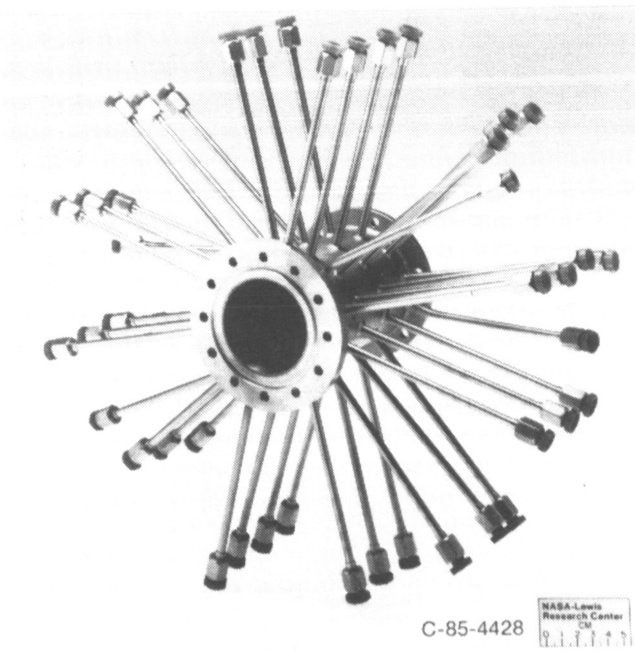

Figure 7.—Calorimeter chamber before instrumentation.

cooling passages. The passages were closed out with a 0.50-cm (0.20-in.) layer of electroformed nickel to form the outer wall of the chamber.

Figure 7 shows the calorimeter chamber before it was instrumented. The calorimeter contained 22 cooling circuits. Each cooling circuit was manifolded with separate inlet and outlet tubes and consisted of two circumferential cooling passages. High-pressure, flexible coolant-water lines connected the vertical pipe manifolds to the cooling circuit connectors, which were welded to the calorimeter chamber. The circumferential cooling passages allowed individual cooling circuit flow control, which resulted in accurate measurement of heat flux for each station on the basis of the coolant-water temperature rise and mass flow rate. Figure 8 shows the calorimeter chamber assembly on the test stand during a hot firing.

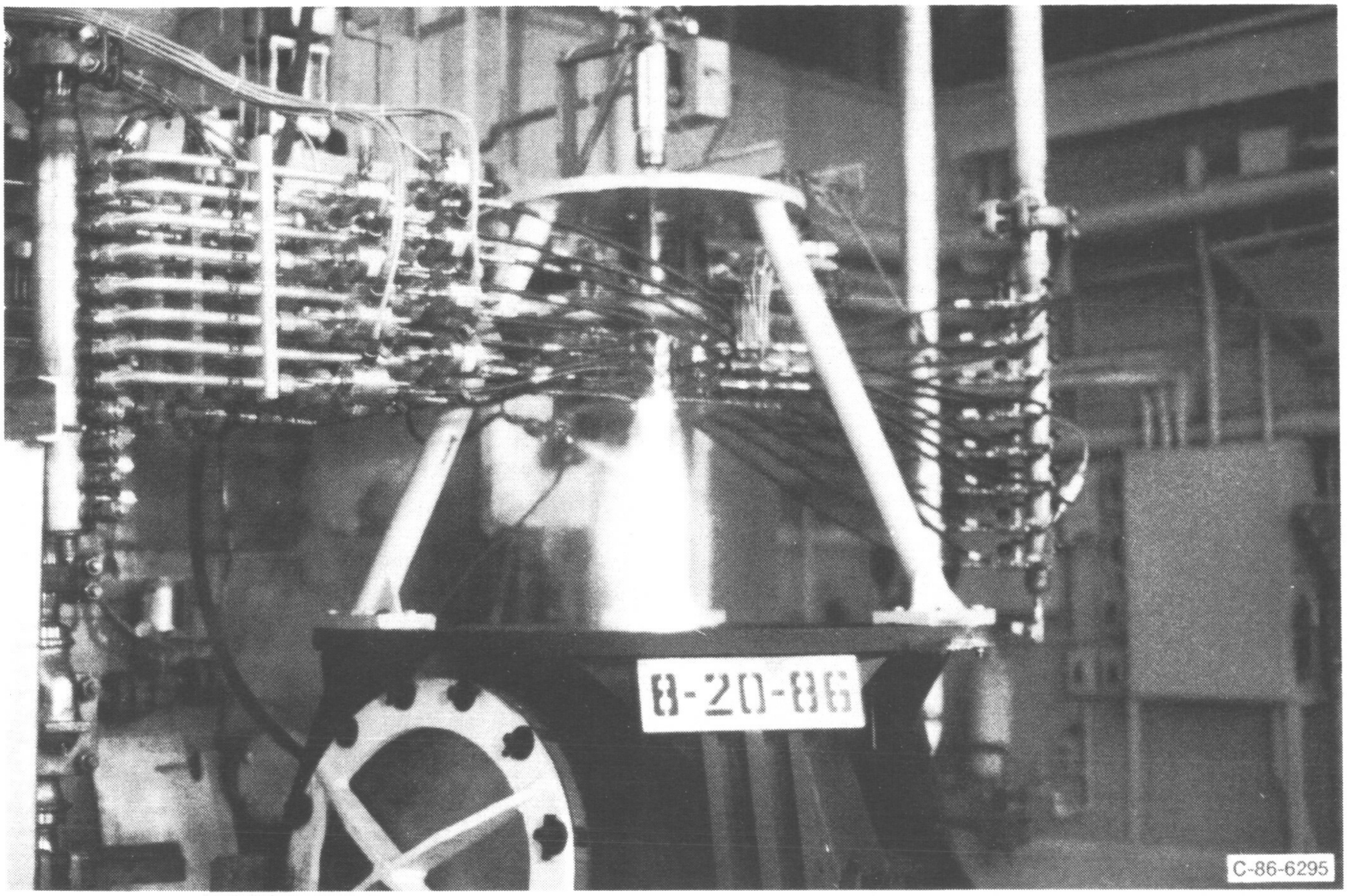

Figure 8.—Calorimeter chamber assembly during hot-fire test.

Instrumentation

The instrumentation on the calorimeter consisted primarily of Chromel/constantan thermocouples and venturi flowmeters. A venturi flowmeter was installed in each coolant inlet tube, and a thermocouple was installed in each coolant outlet tube so that the water mass flow and temperature rise in each cooling circuit could be determined. Two thermocouples were used to measure the coolant-water inlet temperature for the entire system. In addition, the water inlet and outlet pressures were measured.

At 11 of the 22 axial locations thermocouples were set in the cooling passage ribs to determine the hot-gas-side wall temperature. There were four thermocouples, 90° apart, at three axial locations in the throat region and two thermocouples, 180° apart, at the other eight axial locations. The thermocouples were spring loaded against the bottom of the rib holes.

Test Facility

The tests were conducted at the Lewis Research Center Rocket Engine Test Facility. This is a 222-kN (50 000-lbf) sea-level rocket test stand equipped with an exhaust-gas muffler and scrubber. Propellants and coolants are supplied to the test stand from pressurized tanks. The combustion gases and the centerbody coolant water are expelled into the scrubber. Ignition is achieved by using a spark-ignited external torch operating with gaseous hydrogen and gaseous oxygen. The torch is turned on just before the propellants are flowed to the main chamber, thus backlighting the chamber.

All pressures and temperatures were recorded in digital form on a magnetic tape. The digital recording system was set at a basic rate of 5000 samples per second. After processing, all of the data and the calculations performed on the data could be printed out on the control room terminal.

Test Procedure

The experimental calorimeter program consisted of two series of tests. The first series of tests were conducted with the injector having the platelet faceplate. The second series of tests were conducted using the same injector with the Rigimesh faceplate.

In order to replicate the hot-gas-side boundary conditions for the liquid-hydrogen-cooled test chambers, an attempt was made to achieve the same wall temperatures for the water-cooled calorimeter chamber. This could only be done in the throat region, where the coolant-water flow was set to obtain

a hot-gas-side wall temperature of 722 to 777 K (1300 to 1400 °R) at the throat station. This is the desirable maximum operating temperature for combustion chamber liners fabricated from copper-base alloys.

Fixed valve positions were used to set mixture ratio and chamber pressure. The coolant-water flow to the calorimeter was controlled by tank pressure and valve position. Water flow to the centerbody was set to the maximum obtainable and occurred before, during, and after the hot-fire tests. All tests were monitored by closed-circuit television and a test cell microphone. The television and audio outputs were recorded on magnetic tape.

Results and Discussion

Tests were conducted to determine the hot-gas-side heat transfer characteristics for a subscale plug-nozzle rocket chamber by using a water-cooled calorimeter chamber with gaseous hydrogen and liquid oxygen as the propellants. Injector performance and chamber heat transfer data were obtained for two showerhead injector configurations: one with a platelet faceplate and the other with a Rigimesh faceplate. Four tests were conducted with the platelet injector at a nominal chamber pressure of 4.14 MPa abs (600 psia) and a mixture ratio O/F range from 5.8 to 6.1. Three tests were conducted with the Rigimesh injector at a nominal chamber pressure of 4.14 MPa abs (600 psia) and an O/F range from 5.9 to 6.3.

Injector Performance

The injector with the Rigimesh faceplate showed slightly better performance than the injector with the platelet faceplate, having an average characteristic-exhaust-velocity efficiency C^* of 96 percent as compared with 94.4 percent for the platelet faceplate.

Determination of Heat Flux and Hot-Gas-Side Wall Temperature

The total heat flux Q was calculated from the coolant-water temperature rise and the mass flow rate as

$$Q = mC_p\left(T_{ce} - T_{ci}\right) \tag{1}$$

where m is the mass flow rate, C_p is the specific heat of water, T_{ce} is the coolant exit temperature, and T_{ci} is the coolant inlet temperature. The average coolant-water temperature rise for all test runs ranged from 3.3 deg K (6 deg R) in the cooling circuit closest to the injector to 41 deg K (74 deg R) in the cooling circuit at the throat station.

The average heat flux for each station was calculated by

$$q = \frac{Q}{A} \tag{2}$$

where A is the hot-gas-side surface area for the station. Heat-flux profiles are shown for the Rigimesh and platelet faceplates in figure 9. The data points for each of the faceplates lie almost on top of one another, showing little difference from test to test. Both figures show that a step change in the heat flux level occurred at approximately 7 cm (2.76 in.) upstream of the throat, indicating that it took about 3 cm (1.18 in.) to achieve sufficient mixing before rapid burning of the propellants could take place. In order to compare the data for the two faceplates, all of the data for each faceplate were averaged and are shown in figure 10. The results show that the heat flux level near the faceplate was higher for the Rigimesh faceplate than for the platelet faceplate, indicating somewhat better

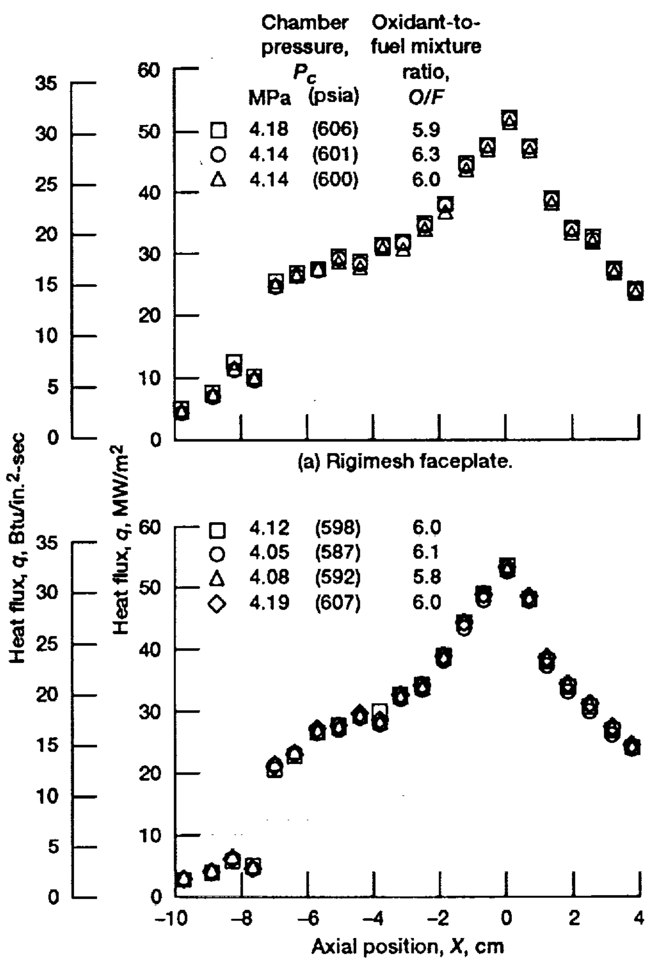

(b) Platelet faceplate.

Figure 9.—Heat flux versus axial position.

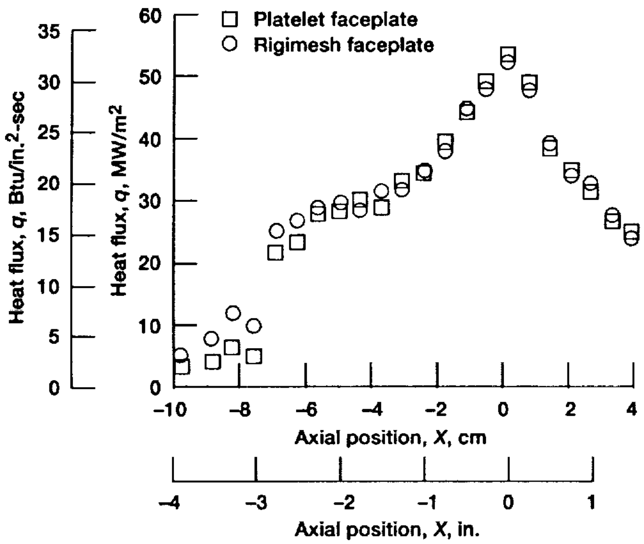

Figure 10.—Averaged heat flux versus axial position.

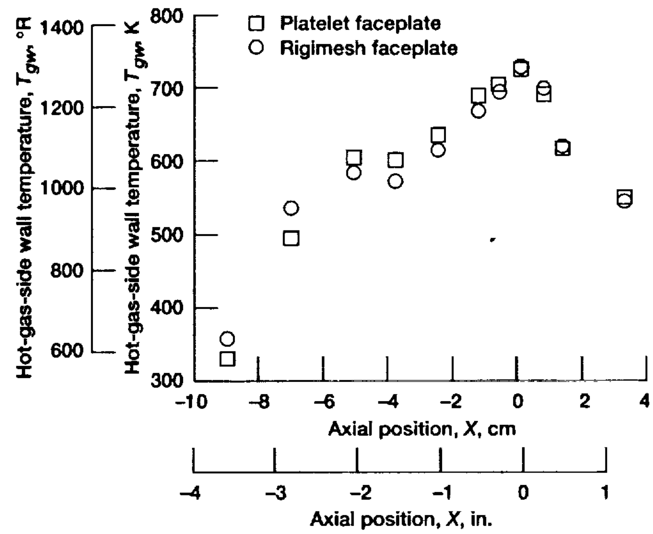

Figure 11.—Averaged hot-gas-side wall temperature versus axial position.

mixing for the Rigimesh faceplate near the injector face. The data for the two faceplates converge at 5.72 cm (2.25 in.) upstream of the throat, which was approximately 2.2 cm (0.87 in.) before the start of the convergence region of the combustion chamber, and show little difference for the remainder of the chamber. The heat flux for the platelet injector reached a maximum of 54 MW/m^2 (33 Btu/in.^{2}-sec) at the throat and was only 2.3 percent higher than that for the Rigimesh faceplate.

Hot-gas-side wall temperatures were calculated from the measured temperatures at the stations that had rib thermocouples. The hot-gas-side wall temperature T_{gw} was calculated from the heat transfer through the metal wall of thickness t by assuming no axial conduction (one-dimensional heat transfer). The wall temperature and the wall material conductivity K were iterated upon until $|(T_{gw})^{m+1} - (T_{gw})^m| < 0.01$. For the first iteration T_{gw} was set equal to the calculated combustion gas static temperature T_s. Then, an average temperature T_{av} was used to calculate the conductivity.

$$T_{av} = 0.5\left[T_{rib} + \left(T_{gw}\right)^m\right] \quad (3)$$

$$K_m = 0.546363 \times 10^{-2} - 0.483916 \times 10^{-6}\ T_{av} \quad (4)$$

From the conductivity K, the rib wall temperature T_{rib}, and the heat flux q, a new wall temperature was calculated as

$$\left(T_{gw}\right)^{m+1} = T_{rib} + \frac{qt}{K} \quad (5)$$

where t is the distance from the rib thermocouple to the hot-gas-side wall. The thermocouples were located in the ribs 0.076 cm (0.03 in.) from the hot-gas-side wall. The average temperature difference between the thermocouple location and the hot-gas-side wall ranged from 6.7 deg K (12 deg R) at station 2 to 108 deg K (195 deg R) at the throat station. The averaged calculated wall temperatures along the chamber length are shown in figure 11 for the two faceplates. Because the heat flux data for the two injectors showed very little variation from run to run, only the averages of the measured and calculated results are shown for each injector for the remainder of the report. The calculated wall temperatures showed the same trend as the heat flux data, with the temperatures from the Rigimesh faceplate being higher near the injector face than the temperatures from the platelet faceplate. The peak average wall temperatures for the two injector faceplates were approximately equal at 730 K (1314 °R) at the chamber throat.

Hot-Gas-Side Heat Transfer Coefficients and Correlation Coefficients

The heat transfer coefficients and hot-gas-side correlation coefficients for a Nusselt number correlation were also calculated from the experimental data. In order to obtain the thermodynamic and transport properties for the heat transfer correlations, the following procedure was used: The combustion temperature T_0 was assumed to vary with the square of the C^* efficiency (i.e., $T_0 = T_{0,theo} \times (C^*)^2$), where $T_{0,theo}$ is the theoretical combustion temperature. The total pressure at the throat $P_{c,cor}$ was determined by correcting the measured chamber pressure at the injector face for the momentum pressure loss MPL. By using $P_{c,cor}$, T_0, and the measured mixture ratio, a one-dimensional isentropic expansion for equilibrium composition was performed (ref. 12) to obtain the combustion total enthalpy i_0 and the static pressure, temperature, and enthalpy for each station.

The heat transfer coefficient h_g is a function of the heat flux and the temperature difference across the hot-gas-side boundary layer,

$$h_{g,T} = \frac{q}{T_{aw} - T_{gw}} \tag{6}$$

where T_{aw} is the adiabatic wall temperature or a function of the enthalpy difference across the boundary layer

$$h_{g,i} = \frac{q}{i_{aw} - i_{gw}} \tag{7}$$

where i_{gw} is hot-gas-side wall enthalpy and i_{aw} is the adiabatic wall enthalpy.

The adiabatic wall enthalpy is calculated from

$$i_{aw} = i_s + (\mathrm{Pr})_r^{1/3} \left(i_0 - i_s\right) \tag{8}$$

where i_0 is the total combustion enthalpy, i_s is the static enthalpy, and $(\mathrm{Pr})_r$ is the reference Prandtl number. The Prandtl number, as well as all of the transport properties used in the correlations, were evaluated at Eckert's reference enthalpy i_r (ref. 13) and the local static pressure.

$$i_r = 0.5 \left(i_s + i_{gw}\right) + 0.22 \, (\mathrm{Pr})_r^{1/3} \left(i_0 - i_s\right) \tag{9}$$

Figure 12 shows the averaged heat transfer coefficients based on enthalpy $h_{g,i}$ as a function of the axial position for the two faceplates. Although the correlation coefficients, which are discussed later in the report, were derived from an enthalpy-based heat transfer coefficient, the averaged heat transfer coefficients based on temperature $h_{g,T}$ are also shown in figure 13.

Using the heat transfer coefficients as a function of enthalpy, the hot-gas-side correlation coefficients were calculated for a Nusselt number type of correlation for fully developed turbulent pipe flow,

$$Nu = \frac{h_g d}{k} = C_g (Re)^{0.8} (Pr)^{0.3} \tag{10}$$

where the transport properties in the Reynolds and Prandtl numbers and the gas conductivity k were evaluated at Eckert's reference enthalpy and the local wall static pressure and d is the hydraulic diameter. Solving for C_g resulted in the following equation:

$$C_g = \frac{h_g d}{k (Re)^{0.8} (Pr)^{0.3}} \tag{11}$$

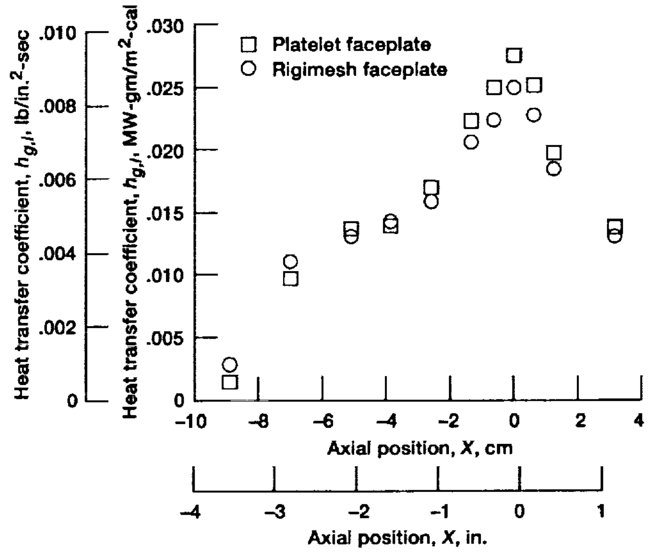

Figure 12.—Averaged heat transfer coefficient based on enthalpy versus axial position.

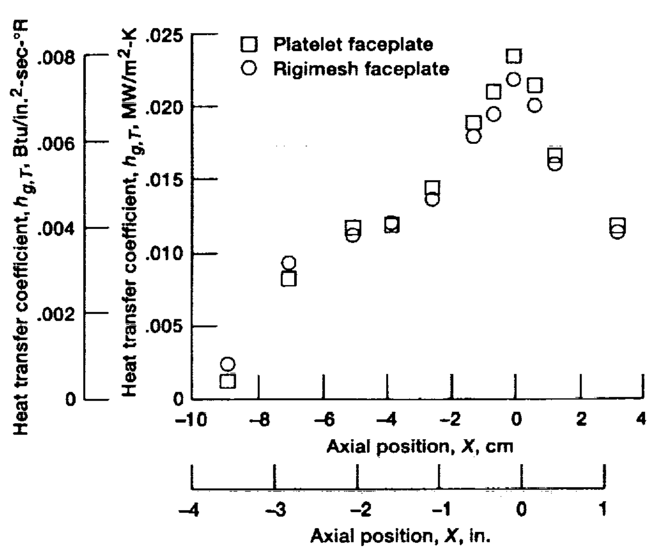

Figure 13.—Averaged heat transfer coefficient based on temperature versus axial position.

For fully developed, turbulent pipe flow in a constant-area duct the value of the constant C_g has been generally found to vary from 0.023 to 0.026. However, it is a well-known fact that C_g is not a constant for turbulent flow in a converging-diverging nozzle. This has been attributed to a reduction in the turbulence intensity as the flow accelerates in the convergent region of the nozzle resulting in a suppression in the value of C_g, with the minimum occurring in the throat region (refs. 14 to 20).

Figure 14 shows the averaged correlation coefficient C_g as a function of axial position for the two injector faceplates. In order to compare the values of C_g relative to that of fully developed, turbulent pipe flow, two lines representing constant

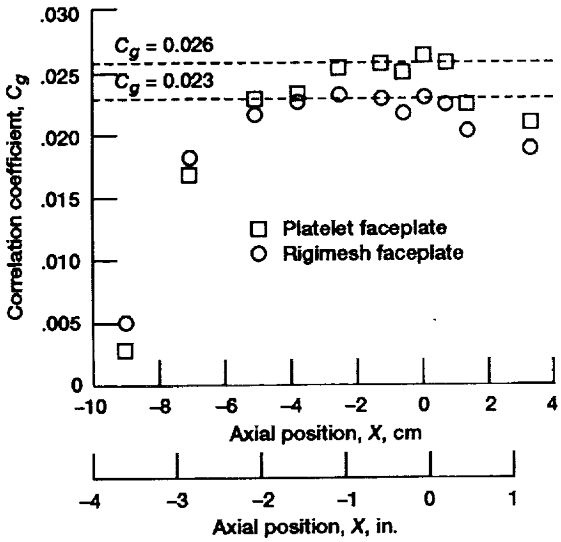

Figure 14.—Averaged correlation coefficient versus axial position. $Nu = C_g(Re)^{0.8}(Pr)^{0.3}$.

values of C_g of 0.023 and 0.026 are shown. It can be seen that the values of C_g were very low near the injector, where the combustion process appeared to be incomplete as previously inferred. The values of C_g continued to rise along the chamber length and reached a level of approximately 0.023 at a point 5.0 cm (1.97 in.) upstream of the throat, which was still in the constant-area region of the combustion chamber. The values of C_g remained fairly constant at 0.023 for the Rigimesh faceplate and reached a constant level of 0.026 for the platelet faceplate to a point just downstream of the throat, where the values started to diminish. The values of C_g did not diminish in the convergent and throat regions of the chamber, which could be due to the low contraction ratio and the small convergent angle upstream of the throat.

Summary of Results

An experimental investigation was conducted to determine the hot-gas-side heat transfer characteristics for a subscale, plug-nozzle rocket test apparatus. In order to obtain the data, a water-cooled calorimeter chamber was tested at a nominal chamber pressure of 4.14 MPa abs (600 psia) over a mixture ratio of 5.8 to 6.3 using gaseous hydrogen and liquid oxygen as the propellants. Two showerhead injectors were evaluated in the test program: one with a Rigimesh faceplate and the other with a platelet faceplate. Heat fluxes and hot-gas-side wall temperatures were obtained along the length of the calorimeter chamber. A summary of the test results is as follows:

1. The Rigimesh and platelet faceplates showed similar performance characteristics, averaging 96.0 percent and 94.4 percent characteristic-exhaust-velocity efficiency, respectively.
2. The heat-flux and temperature profiles for the two injector faceplates were similar. A maximum heat flux of 54 MW/m^2 (33 Btu/in.^{2}-sec) occurred at the throat at a temperature of 730 K (1314 °R) for the platelet faceplate.
3. The throat region correlation coefficient C_g for a Nusselt number correlation of the form $Nu = C_g(Re)^{0.8}(Pr)^{0.3}$ averaged 0.023 for the Rigimesh faceplate and 0.026 for the platelet faceplate.

National Aeronautics and Space Administration
Lewis Research Center
Cleveland, Ohio 44135
February 12, 1993

Appendix – Symbols

A wall surface area

A_t throat flow area

C^* characteristic exhaust velocity, $P_{c,\mathrm{cor}} A_t g/w$

C_g correlation coefficient

C_p specific heat

CR chamber-to-throat contraction ratio

d hydraulic diameter

g gravitational constant

h_g heat transfer coefficient

$h_{g,i}$ heat transfer coefficient based on enthalpy

$h_{g,T}$ heat transfer coefficient based on temperature

I_1 specific impulse at nozzle entrance

i_{aw} adiabatic wall enthalpy

i_{gw} hot-gas-side wall enthalpy

i_r Eckert's reference enthalpy

i_s wall static enthalpy

i_0 experimental combustion total enthalpy

K wall material conductivity

k gas conductivity

MPL momentum pressure loss,

$$P_{\mathrm{inj}} - P_1 = P_{c,\mathrm{cor}} \frac{I_1 g - V_{\mathrm{inj}}}{C^* \mathrm{CR}}$$

m mass flow rate

Nu Nusselt number

O/F oxidant-to-fuel mixture ratio

P_c chamber pressure

$P_{c,\mathrm{cor}}$ chamber pressure corrected for momentum pressure loss

P_{inj} chamber pressure at injector face

P_1 static pressure at nozzle entrance

Pr Prandtl number

Q total heat flux

q heat flux per unit area

Re Reynolds number

T_{av} average wall temperature

T_{aw} adiabatic wall temperature

T_{ce} coolant exit temperature

T_{ci} coolant inlet temperature

T_{gw} hot-gas-side wall temperature

T_{rib} rib wall temperature

T_s combustion gas static temperature

T_0 experimental combustion total temperature

$T_{0,\mathrm{theo}}$ theoretical combustion total temperature

t wall thickness

V_{inj} average velocity of propellants at injector face

w propellant mass flow rate

X axial position

References

1. Carlile, J.A.; and Quentmeyer, R.J.: An Experimental Investigation of High-Aspect-Ratio Cooling Passages. AIAA Paper 92-3154, July 1992. (Also NASA TM-105679, 1992.)
2. Pavli, A.J.; Kazaroff, J.M.; and Jankovsky, R.S.: Hot-Fire Fatigue Testing Results for the Compliant Combustion Chamber. NASA TP-3223, 1992.
3. Kazaroff, J.M.; Jankovsky, R.S.; and Pavli, A.J.: Hot-Fire Test Results of Subscale Tubular Combustion Chambers. NASA TP-3222, 1992.
4. Kazaroff, J.M; and Jankovsky, R.S.: Cyclic Hot Firing Results of Tungsten Reinforced Copper Liner Thrust Chambers. NASA TM-4214, 1990.
5. Quentmeyer, R.J.: Thrust Chamber Thermal Barrier Coating Techniques. Application of Advanced Material for Turbomachinery and Rocket Propulsion. AGARD, Application of Advanced Material for Turbomachinery and Rocket Propulsion, AGARD CP-449, 1989, pp. 18-1 to 18-10. (Also NASA TM-100933, 1988.)
6. Badlani, M.L., et al.: Development of a Simplified Procedure for Rocket Engine Thrust Chamber Life Prediction With Creep. (ODAI-1512-11-83, O'Donnell and Associates, Inc., NASA Contract NAS3-23343), NASA CR-168261, 1983.
7. Porowski, J.S., et al.: Development of a Simplified Procedure for Thrust Chamber Life Prediction. (ODAI-1403-12-81, O'Donnell and Associates, Inc., NASA Contract NAS3-22649), NASA CR-165585, 1981.
8. Quentmeyer, R.J.; Kasper, H.J.; and Kazaroff, J.M.: Investigation of the Effect of Ceramic Coatings of Rocket Thrust Chamber Life. AIAA Paper 78-1034, July 1978. (Also NASA TM-78892, 1978.)
9. Quentmeyer, R.J.: Experimental Fatigue Life Investigation of Cylindrical Thrust Chambers. AIAA Paper 77-893, July 1977. (Also NASA TM X-73665, 1977.)
10. Armstrong, W.H.; and Brogren, E.W.: Thrust Chamber Life Prediction, Volume II, Plug Nozzle Centerbody and Cylinder Life Analysis. (Boeing Aerospace Co., NASA Contract NAS3-17838), NASA, CR-134822, 1975.
11. Mueggenburg, H.; and Repas, G.: A Highly Durable Injector Faceplate Design Concept for O_2/H_2 Propellants. AIAA Paper 90-2181, July 1990.
12. Gordon, S.; and McBride, B.J.: Computer Program for Calculation of Complex Chemical Equilibrium Compositions, Rocket Performance, Incident and Reflected Shocks, and Chapman-Jouguet Detonations. NASA SP-273, 1976.
13. Eckert, E.R.G.; and Drake, R.M., Jr.: Heat and Mass Transfer. Second ed., McGraw-Hill Book Co., Inc., 1959.
14. Back, L.H.; Cuffel, R.F.; and Massier, P.F.: Laminarization of a Turbulent Boundary Layer in Nozzle Flow—Boundary Layer and Heat Transfer Measurements With Wall Cooling. J. Heat Transfer, vol. 92, no. 3, Aug. 1970, pp. 333-334. (Also ASME Paper 69-HT-56, 1969.)
15. Von Glahn, U.H.: Correlation of Gas-Side Heat Transfer for Axisymmetric Rocket Engine Nozzles. NASA TM X-1748, 1969.
16. Boldman, D.R.; Schmidt, J.F.; and Gallagher, A.K.: Laminarization of a Turbulent Boundary Layer as Observed From Heat-Transfer and Boundary-Layer Measurements in Conical Nozzles. NASA TN D-4788, 1968.
17. Boldman, D.R.; Schmidt, J.F.; and Ehlers, R.C.: Effect of Uncooled Inlet Length and Nozzle Convergence Angle on the Turbulent Boundary Layer and Heat Transfer in Conical Nozzles Operating With Air. J. Heat Transfer, vol. 89, no. 4, Nov. 1967, pp. 341-350. (Also ASME Paper 67-HT-28, 1967.)
18. Schacht, R.L.; Quentmeyer, R.J.; and Jones, W.L.: Experimental Investigation of Hot-Gas Side Heat-Transfer Rates for a Hydrogen-Oxygen Rocket. NASA TN D-2832, 1965.
19. Moretti, P.M.; and Kays, W.M.: Heat Transfer to a Turbulent Boundary Layer With Varying Free-Stream Velocity and Varying Surface Temperature—An Experimental Study. Int. J. Heat Mass Transfer, vol. 8, no. 9, Sept. 1965, pp. 1187-1202.
20. Back, L.H.; Massier, P.F.; and Gier, H.L.: Convective Heat Transfer in a Convergent-Divergent Nozzle. Int. J. Heat Mass Transfer, vol. 7, no. 5, May 1964, pp. 549-568.

REPORT DOCUMENTATION PAGE

Form Approved
OMB No. 0704-0188

1. AGENCY USE ONLY (*Leave blank*)	2. REPORT DATE	3. REPORT TYPE AND DATES COVERED
	July 1993	Technical Paper

4. TITLE AND SUBTITLE

Hot-Gas-Side Heat Transfer Characteristics of Subscale, Plug-Nozzle Rocket Calorimeter Chamber

5. FUNDING NUMBERS

WU-584-03-11

6. AUTHOR(S)

Richard J. Quentmeyer and Elizabeth A. Roncace

7. PERFORMING ORGANIZATION NAME(S) AND ADDRESS(ES)

National Aeronautics and Space Administration
Lewis Research Center
Cleveland, Ohio 44135-3191

8. PERFORMING ORGANIZATION REPORT NUMBER

E-7614

9. SPONSORING/MONITORING AGENCY NAMES(S) AND ADDRESS(ES)

National Aeronautics and Space Administration
Washington, D.C. 20546-0001

10. SPONSORING/MONITORING AGENCY REPORT NUMBER

NASA TP-3380

11. SUPPLEMENTARY NOTES

Richard J. Quentmeyer, Sverdrup Technology, Inc., Lewis Research Center Group, 2001 Aerospace Parkway, Brook Park, Ohio 44142. Elizabeth A. Roncace, NASA Lewis Research Center. Responsible person, Richard J. Quentmeyer, (216) 433-7471.

12a. DISTRIBUTION/AVAILABILITY STATEMENT

Unclassified - Unlimited
Subject Category 20

12b. DISTRIBUTION CODE

13. ABSTRACT *(Maximum 200 words)*

An experimental investigation was conducted to determine the hot-gas-side heat transfer characteristics for a liquid-hydrogen-cooled, subscale, plug-nozzle rocket test apparatus. This apparatus has been used since 1975 to evaluate rocket engine advanced cooling concepts and fabrication techniques, to screen candidate combustion chamber liner materials, and to provide data for model development. In order to obtain the data, a water-cooled calorimeter chamber having the same geometric configuration as the plug-nozzle test apparatus was tested. It also used the same two showerhead injector types that have been used on the test apparatus: one having a Rigimesh faceplate and the other having a platelet faceplate. The tests were conducted using liquid oxygen and gaseous hydrogen as the propellants over a mixture ratio range of 5.8 to 6.3 at a nominal chamber pressure of 4.14 MPa abs (600 psia). The two injectors showed similar performance characteristics with the Rigimesh faceplate having a slightly higher average characteristic-exhaust-velocity efficiency of 96 percent versus 94.4 percent for the platelet faceplate. The throat heat flux was 54 MW/m^2 (33 $Btu/in.^2$-sec) at the nominal operating condition, which was a chamber pressure of 4.14 MPa abs (600 psia), a hot-gas-side wall temperature of 730 K (1314 °R), and a mixture ratio of 6.0. The chamber throat region correlation coefficient C_g for a Nusselt number correlation of the form $Nu = C_g(Re)^{0.8}(Pr)^{0.3}$ averaged 0.023 for the Rigimesh faceplate and 0.026 for the platelet faceplate.

14. SUBJECT TERMS

Heat transfer; Rockets; Combustion; Rocket injectors

15. NUMBER OF PAGES

16

16. PRICE CODE

A03

17. SECURITY CLASSIFICATION OF REPORT	18. SECURITY CLASSIFICATION OF THIS PAGE	19. SECURITY CLASSIFICATION OF ABSTRACT	20. LIMITATION OF ABSTRACT
Unclassified	Unclassified	Unclassified	

NSN 7540-01-280-5500

Standard Form 298 (Rev. 2-89)
Prescribed by ANSI Std. Z39-18
298-102